

Unstable dynamics, nonequilibrium phases, and criticality in networked excitable media

S. de Franciscis, J. J. Torres, and J. Marro

Departamento de Electromagnetismo y Física de la Materia, Institute Carlos I for Theoretical and Computational Physics, University of Granada, Granada, Spain

(Received 25 July 2010; published 7 October 2010)

Excitable systems are of great theoretical and practical interest in mathematics, physics, chemistry, and biology. Here, we numerically study models of excitable media, namely, networks whose nodes may occasionally be dormant and the connection weights are allowed to vary with the system activity on a short-time scale, which is a convenient and realistic representation. The resulting global activity is quite sensitive to stimuli and eventually becomes unstable also in the absence of any stimuli. Outstanding consequences of such unstable dynamics are the spontaneous occurrence of various *nonequilibrium* phases—including *associative-memory* phases and one in which the global activity wanders irregularly, e.g., chaotically among all or part of the dynamic attractors—and $1/f$ noise as the system is driven into the phase region corresponding to the most irregular behavior. A net result is resilience which results in an efficient search in the model attractor space that can explain the origin of some observed behavior in neural, genetic, and ill-condensed matter systems. By extensive computer simulation we also address a previously conjectured relation between observed power-law distributions and the possible occurrence of a “critical state” during functionality of, e.g., cortical networks, and describe the precise nature of such criticality in the model which may serve to guide future experiments.

DOI: [10.1103/PhysRevE.82.041105](https://doi.org/10.1103/PhysRevE.82.041105)

PACS number(s): 05.40.-a, 89.75.Hc, 84.35.+i, 05.45.-a

I. INTRODUCTION

A network is said to have attractors when it can autonomously change its pattern of overall activity to converge with time toward one case while being resilient to perturbations. Following psychological observations [1] and theoretical work [2,3], the concept was popular two decades ago as a mathematical tool to explore the fundamentals of brain tasks attributed to cooperation between many neurons. According to the, say, *standard model* [4], patterns of information, corresponding to sets of values for the nodes activity, are stored in a way that affects the intensities of the edges, representing synapses, which induce a heterogeneous distribution of the edge weights. The global activity may then converge toward one of the given patterns when starting with a degraded version of it. That is, the system exhibits kind of resilience, often known as *associative memory*—a property that mimics the process of recognizing a childhood friend we have not seen for dozens of years—which, being common to humans, is difficult to efficiently emulate with computers. Such a remarkable consequence of cooperation is also relevant to the understanding of complexity in a variety of systems and to solve actual optimization problems [2,4–7].

The systems of interest in nature not only choose eventually one out of a set of patterns and stay *ad infinitum* in its neighborhood but also exhibit an extremely difficult bizarre dynamic behavior (see [8–10] and references therein). For example, signals from the heart and cortical neural activities have been successfully interpreted using nonlinear dynamic theory [11–18], and the standard model has been generalized along biologically motivated lines that endow it with even more interesting behavior [19–26]. In particular, it was shown that one may capture some of the observed shaky mechanisms and instabilities by taking into account two features that seem to characterize generically excitable media [27], namely, assuming both rapid activity-dependent fluctuations

of the edge weights and the existence of nodes that are reluctant to a change of state during a time interval after operation. It is remarkable that incorporating these simple mechanisms into the standard model has allowed one to recreate [28] the transient dynamics of activity as observed in experiments concerning the locust odor representation [29].

Instead of just associative memory, one may readily identify in this experiment, as in most of the available observations (e.g., the ones mentioned in the previous paragraph) a kind of continuous and irregular wandering among attractors, say, *roaming dynamics*. The nervous system is definitely not the only network that exhibits both varying edge weights and silent nodes at a basic level of observation and, as a reflection of this at a higher level, this sort of roaming dynamics. This occurs in ill-condensed matter, for instance, whose emerging properties are determined by “microscopic disorder.” In fact, it is sensible to imagine such a disorder is more involved than assumed in familiar spin-glass models. That is, the effective interactions between ions should certainly be expected to have short-time variations—associated with ion diffusion, basic chemical reactions, and other local changes concerning impurities, misfits, fields, rearrangements, strains, etc.—which would, in general, induce nonequilibrium patterns of activity as, for example, observed in reaction-diffusion systems [30,31]. It is likely that the behavior of genetic networks during biological evolution is another case of microscopically induced roaming dynamics [32–34]. Furthermore, though to our knowledge the relevance of roaming has not yet been described for other excitable systems, it is noticeable that variability of connections and occasional lack of individual activity are features that typically characterize friendship, social, professional, and business contacts [35], as well as the case of the interrelated metabolic reactions that run the cell, food webs, and transport and communication networked systems, for instance.

In this paper, we describe in detail model phenomenology bearing relevance to situations with spontaneously unstable

dynamics associated with excitability as described in the two previous paragraphs. By extensive computer simulations, we show both first- and second-order phase transitions, characterize the nature of different *nonequilibrium phases* [30] that occur as one modifies the system parameters, study the details of the network activity dynamics, and determine the conditions in which long-range correlations and non-Gaussian noise emerge. This results in a systematic study that adds up to recent efforts trying to understand the origin of the observed relation between certain statistical criticality and dynamically critical functionality in neuroscience [9,10,36–42]. Our study in this paper complements analytical study of the simplest limits of the same model in Ref. [27] and related exploratory numerical studies therein.

II. DEFINITION OF MODEL

Consider a network in which the consequences of the activity changes of each node above threshold may be sketched by means of a binary variable: $\sigma_i = \pm 1$, $i = 1, \dots, N$. This is known to suffice in practice to investigate main effects of cooperation in different contexts [43]. Each node receives a signal—alternatively, endures a local field— $h_i(\sigma) = \sum_{j \neq i} w_{ij} \sigma_j$, where $\sigma = \{\sigma_i\}$ stands for the global activity and w_{ij} is the weight of the connection between nodes i and j . In the problems of interest, one may typically single out P patterns of activity, namely, $\{\xi_i^\mu = \pm 1\}$ with $\mu = 1, \dots, P$, which have some special relevance. The weights then follow accordingly, e.g., by means of the superposition rule $w_{ij} = \frac{1}{N} \sum_{\mu=1}^P \xi_i^\mu \xi_j^\mu$. This is one of the simplest conditions that transforms the special P patterns into attractors of dynamics [1,4].

Short-time variability of connections will be introduced by assuming that their weights are given by $\bar{w}_{ij} = \epsilon_j w_{ij}$, where ϵ_j is a stochastic variable. In order to mimic the cases of interest, this variable should change very rapidly compared with the network characteristic time scale. Therefore, we shall assume that it can be described by a stationary distribution. This is taken here as $P_{st}(\epsilon_j | \sigma) = \zeta(\sigma) \delta(\epsilon_j - \Phi) + [1 - \zeta(\sigma)] \delta(\epsilon_j - 1)$. That is, with probability $\zeta(\sigma)$, which in general depends on the global network activity, the weights are changed by a factor Φ but remain unchanged otherwise. Depending on the value of Φ , this may simulate node excitability, potentiation, or fatigue of the connections as a function of the degree of order in the system. The standard model corresponds to $\Phi = 1$. Other choices for $P_{st}(\epsilon_j | \sigma)$ have been investigated [44], including one in which the weights change depending on the degree of local order, and it seems that these details do not modify essentially the system behavior. We shall assume here for simplicity that the relevant probability in P_{st} is the order parameter,

$$\zeta(\sigma) = \zeta(\mathbf{m}) \equiv \frac{1}{1 + P/N} \sum_{\mu=1}^P [m^\mu(\sigma)]^2. \quad (1)$$

Here, $\mathbf{m} = \{m^1(\sigma), \dots, m^P(\sigma)\}$ is a vector whose components are the P overlaps of the current state σ with each of the singularized patterns, namely, $m^\mu(\sigma) = \frac{1}{N} \sum_{i=1}^N \sigma_i \xi_i^\mu$.

Time evolution is a consequence of transitions $\sigma_i \rightarrow \pm \sigma_i$ that we performed with probability $\frac{1}{2} \{1 - \sigma_i \tanh[h_i(\sigma) T^{-1}]\}$.

Here, T is a parameter that measures the degree of stochasticity driving the evolution—the so-called network *temperature*. Another main parameter is the fraction, ρ , of nodes which is updated at each unit of time or MCS—the Monte Carlo step (per node). For simplicity, we shall assume here these nodes chosen at random from the whole set of N . In this way, the result is a situation in between the limits $\rho \rightarrow 0$ (sequential or *Glauber updating*) and $\rho \rightarrow 1$ (parallel or *Little updating*). The case of intermediate ρ better corresponds to those situations in which due to excitability or other causes, e.g., power economy, not all the elements are active at all times.

For simplicity, we shall be concerned only with mutually orthogonal patterns. This is achieved in practice setting every node in ξ_i^μ for all μ equal to $+1$ or -1 independently with the same probability, so that $\xi_i^\mu \cdot \xi_i^\nu \approx 0$ for any $\mu \neq \nu$ in a large system. (Assuming specific sets of P correlated patterns, which is of great practical interest, is beyond the scope of this paper that intentionally understates this model detail.) Then, under some restrictions which strictly require also the limit $\rho \rightarrow 0$ (see [45] for technical details), the conditions so far stated may be taken into account by assuming *effective weights*,

$$\bar{w}_{ij} = \left\{ 1 - \frac{1 - \Phi}{2} [\zeta(\mathbf{m}) + \zeta(\mathbf{m}^i)] \right\} w_{ij}, \quad (2)$$

where the components of \mathbf{m}^i are $m^\mu(\sigma) - 2\sigma_i \xi_i^\mu N^{-1}$. We shall consider in the following this simplified version of our model which coincides with the general case for any $\rho > 0$ after averaging $\bar{w}_{ij} = \epsilon_j w_{ij}$ over the stationary noise distribution $P_{st}(\epsilon_j | \sigma)$. As a matter of fact, Eq. (2) may formally be viewed as any learning prescription, w_{ij} , which is affected by a multiplicative noise—with correlations built due to the dependence on \mathbf{m} . Incidentally, connections that are roughly of this type were recently shown to induce sort of criticality in (neural) population dynamics [46].

III. PHASES AND DIAGRAMS

A main observation concerns the nature of the phases exhibited as one varies the noise parameter Φ , the fraction of active nodes ρ , the temperature T , and the load parameter $\alpha = P/N$. It turns out convenient to monitor the time evolution of various order parameters [47,48], in particular,

$$M = \langle |\bar{m}^*| \rangle = \frac{1}{N} \left\langle \left| \sum_i \xi_i^* \sigma_i \right| \right\rangle, \quad (3)$$

where the asterisk is the value of μ that identifies the pattern having the largest squared overlap, $(m^*)^2$, and $\langle \dots \rangle$ and $\langle \dots \rangle$ stand for averages over time and over independent realizations of the experiment, respectively (i.e., changing both the initial conditions and the set of the special stored patterns). The set of the other overlaps, m^μ with $\mu \neq *$, may be characterized by

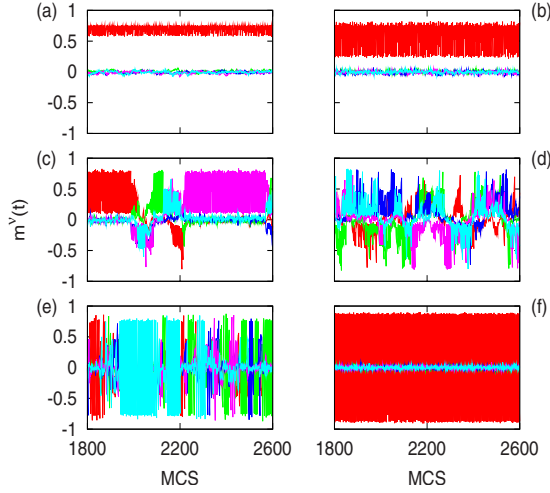


FIG. 1. (Color online) The overlap functions $m^\nu(t)$ showing typical different behaviors for $N=1600$ nodes, $P=5$ patterns, noise parameter $\Phi=-0.5$, temperature $T=0.01$, and, from top to bottom, associative memory as in \mathbf{Ph}_1 at (a) $\rho=0.10$ (left) and (b) $\rho=0.30$ (right); irregular roaming among patterns at (c) $\rho=0.375$ (left) and (d) $\rho=0.40$ (right) as in \mathbf{Ph}_4 ; eventual jumping between patterns after a set of oscillations between a pattern and its negative (*antipattern*) as in \mathbf{Ph}_5 at (e) $\rho=0.50$ (left); and pure pattern-antipattern oscillations as in \mathbf{Ph}_6 at (f) $\rho=0.60$. (Different colors or gray intensities correspond to different values of ν .)

$$R = \frac{1}{1 + \alpha} \left\langle \frac{\sum_{\mu \neq *}}{(m^\mu)^2} \right\rangle, \quad (4)$$

where the sum is over all patterns excluding the one in Eq. (3). We also monitored the global activity by means of

$$Q = \frac{1}{N} \left\langle \sum_i \bar{\sigma}_i^2 \right\rangle. \quad (5)$$

Our values for M , R , and Q in the following involve sufficient averages of independent values to obtain smooth typical behavior, namely, from 200 to 1000 MCS and 50–100 systems for static values and from 10 000 to 50 000 MCS and 10 systems for time-dependent values, unless indicated otherwise.

In the standard case $\Phi=1$, for uncorrelated patterns, the system shows three phases [4,47]:

(\mathbf{Ph}_1) *Memory phase*, in which the system evolves toward one of the given patterns—often known as *pure* or *Mattis states*. The stationary state corresponds to maximum overlap with the particular pattern, so that M is large while R is small in the stationary state, namely, $R \sim \mathcal{O}[(P-1)/(N+P)]$. One also has that $Q \approx 1$ near $T=0$. (This case is illustrated by the two top graphs in Fig. 1.)

(\mathbf{Ph}_2) *Mixture phase*, in which a large system converges to a mixture of pure states, so that it exhibits some order but not associative memory. Therefore, one may have several relatively large overlaps, which induce that $0 < M < 1$ with a lower bound—due to finite size—on the order of $1/\sqrt{N}$, while $0 < R < (P-1)/(1+\alpha)$ with a lower bound on the order of $(P-1)/(N+P)$. Also, $Q \approx 1$ near $T=0$.

(\mathbf{Ph}_3) *Disordered phase*, in which the system remains

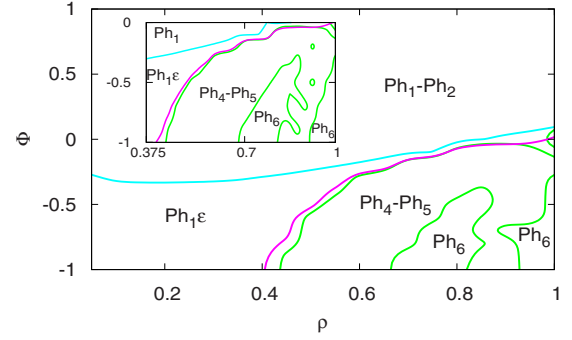


FIG. 2. (Color online) Nonequilibrium phase diagram (Φ, ρ) at low temperature. This was obtained for $N=1600$, $P=5$, and $T=0.1$ from detailed analysis of all the order-parameter functions. The top (blue) line is for $M=0.8$. This leaves the equilibrium phases above, where \mathbf{Ph}_1 occurs with probability 0.87 and \mathbf{Ph}_2 otherwise. To the bottom, the next (violet) line—leaving also $\mathbf{Ph}_1\epsilon$ above—is for $M=0.5$. The next (green) lines comprise an inverted U-shaped region in which $R > 0.18$. The inset shows the roaming region in more detail.

completely disordered as dominated by thermal noise. Then, all the overlaps oscillate around zero, so that $M \sim \mathcal{O}(1/\sqrt{N})$ and R is on the order of $(P-1)/(N+P)$ and $Q \approx 0$ in the stationary state.

These cases correspond, respectively, to the familiar ferromagnetic, spin-glass and paramagnetic phases that are well characterized in studies of equilibrium magnetic models.

The behavior of our system is more complex than suggested by this picture, however. A main novelty for $\Phi \neq 1$ is that, as illustrated in Fig. 1, the system exhibits different types of dynamic behavior that cannot be fitted to the above. That is, one observes that dynamics may eventually destabilize in such a way that quite irregular jumping—among attractors as well as from one pattern to its negative (*antipattern*)—occurs. The observed behavior suggests one to define the following dynamic scenarios, say, nonequilibrium phases that do not occur in the standard model.

(\mathbf{Ph}_4) *Irregular roaming*, in which the activity keeps randomly visiting the basins of attraction corresponding to different patterns. [This is the case in Figs. 1(c) and 1(d), i.e., the two middle graphs in Fig. 1.]

(\mathbf{Ph}_5) *Irregular roaming as for \mathbf{Ph}_4 but eventually interrupted at random during some time by oscillations between a pattern and its antipattern*. [This occurs in Fig. 1(e).]

(\mathbf{Ph}_6) *Pure pattern-antipattern oscillations*. [As in Fig. 1(f).]

These three genuine nonequilibrium cases correspond to $Q \approx 0$ and $M \approx 0$ (due to orthogonality). Case \mathbf{Ph}_6 also has $R \approx 0$ (revealing the symmetry of oscillations), while both \mathbf{Ph}_4 and \mathbf{Ph}_5 have $R \neq 0$. In order to properly characterize these dynamic cases, we shall monitor latter the statistics of the itinerant trajectory.

The different behaviors are better observed and interpreted at very low temperature. As shown in Fig. 2, the disordered phase \mathbf{Ph}_3 is not observed at the chosen (low) temperature, while the ordered, ferromagnetic, and spin-glass phases then occur for any Φ as far as ρ is not too large. That is, one may have familiar order as in equilibrium—

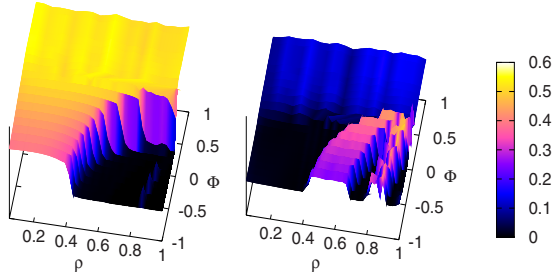


FIG. 3. (Color online) $M(\Phi, \rho)$ (left) and $R(\Phi, \rho)$ (right) for $N = 1600$, $P = 5$, and $T = 0.1$. There is coexistence of \mathbf{Ph}_1 and \mathbf{Ph}_2 for $\Phi > 0$, while the latter phase does not show up for $\Phi < 0$ and memory then occurs but as $\mathbf{Ph}_1\epsilon$ (see the main text) at sufficiently low ρ .

practically independently (over a wide range) of the noise affecting the connections—as far as only a relatively small fraction of nodes are simultaneously active [45]. However, one observes small fluctuations or dispersion with time around the mean value M and that the amplitude of this kind of “error” increases as one lowers Φ and increases ρ . This effect, which is evident when one compares the two top panels in Fig. 1, led us to indicate a zone $\mathbf{Ph}_1\epsilon$ around the region for $\Phi < 0$ and $\rho \leq 0.5$. It is worth distinguishing this zone which reveals how the ferromagnetic phase \mathbf{Ph}_1 has resilience, i.e., a remarkable stability of the attractor to large fluctuations. These increase monotonously with increasing ρ and/or decreasing further Φ , and it finally results in jumping to other attractors (as in the two middle graphs in Fig. 1) when more than one half of the nodes are simultaneously active or, say, synchronized. This is the origin of the genuine nonequilibrium cases \mathbf{Ph}_4 , \mathbf{Ph}_5 , and \mathbf{Ph}_6 . In fact, as shown in Fig. 2, one observes the onset of irregular roaming with $R \neq 0$ and $M = 0$ for $\Phi < 0$ and ρ between 0.4 and 0.6.

The above picture and Fig. 2 follow from a detailed combined analysis of functions $M(\Phi, \rho)$, $R(\Phi, \rho)$, and $Q(\Phi, \rho)$, as illustrated in Fig. 3. This also shows that two main types of phase transitions between equilibrium and nonequilibrium phases occur (see Fig. 4). There is a second-order or continuous transition, as one maintains $\Phi < 0$ at a constant value from the memory phase with large error, i.e., $\mathbf{Ph}_1\epsilon$, to the

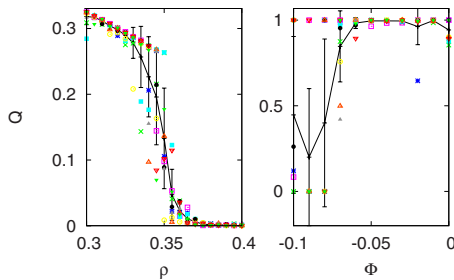


FIG. 4. (Color online) Left: Second-order phase transition between $\mathbf{Ph}_1\epsilon$ and \mathbf{Ph}_4 around $\rho \approx 0.37$ when $\Phi = -0.8$. Right: first-order phase transition between \mathbf{Ph}_1 and \mathbf{Ph}_5 around $\Phi = -0.1$ when $\rho = 0.8$. Both plots are for $N = 1600$, $P = 5$, and $T = 0.01$. Note that different realizations using a different seed produce here different values corresponding to the different symbols; the mean of all the realizations is represented by a solid curve.

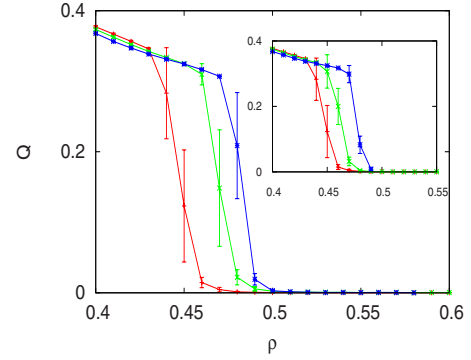


FIG. 5. (Color online) The second-order phase transition on the left of Fig. 4. For the same system as in this figure, the main graph here shows data for $P = 5$ and $N = 1600$, 3200 , and 6400 , respectively from left to right in the middle of the Q value. The inset is for the same values of N but $P = 5$, 10 , and 20 , respectively, i.e., same value of α .

irregular roaming phase \mathbf{Ph}_4 . Then, at least near $T = 0$, one also observes a first-order or discontinuous transition (Fig. 4), as ρ is maintained constant, from the memory phase to the irregular roaming with pattern-antipattern oscillations, namely, \mathbf{Ph}_5 . Furthermore, it is noticeable here that, as illustrated in Fig. 5, the transition region depends on the value of $\alpha = P/N$, that is, the critical value of ρ increases somewhat with decreasing α for finite N , and it seems to go to $\rho \approx 0.5$ as $N \rightarrow \infty$ for finite α .

The rare shape of the roaming region in plane (Φ, ρ) for $P = 5$, which shows in detail the inset of Fig. 2, is roughly the same as the one obtained analytically when $P = 1$ for the change of sign of the Lyapunov exponent in a closely related model (Fig. 2 in Ref. [27]). This confirms the general observation during our MC experiments of kind of chaos within the inverted-U region which is delimited in Fig. 2 by green lines. That is, one should endow a chaotic character to the roaming region. That similarity also reinforces the reliability of our measures of order, and it shows how robust the model here is in relation to the dynamically irregular behavior. It also follows, in particular, that the model parameter P is irrelevant to this qualitative behavior at least as long as not too many patterns are stored.

The “phases” \mathbf{Ph}_4 and \mathbf{Ph}_5 , e.g., cases (d) and (e) in Fig. 1, cannot be discriminated on the basis of M , R , and Q only. The top panel in Fig. 6 illustrates how these functions change with ρ for fixed Φ at low temperature. The bottom panel illustrates the dynamic transition from irregular roaming in \mathbf{Ph}_4 to the more regular behavior in \mathbf{Ph}_5 as a consequence of increasing the amplitude of fluctuations around the attractor as the fraction ρ of active nodes is increased during time evolution. As indicated in Fig. 2, the separation between the memory phase \mathbf{Ph}_1 or $\mathbf{Ph}_1\epsilon$ and the nonequilibrium cases is clear cut, while again it results more difficult to discriminate numerically the region \mathbf{Ph}_6 of pure pattern-antipattern oscillations (where $M = R = 0$) out of the \mathbf{Ph}_4 – \mathbf{Ph}_5 chaotic region (where $M = Q = 0$ with $R \neq 0$). In any case, however, our finding concerning this agrees with the analytical result in a related case [27].

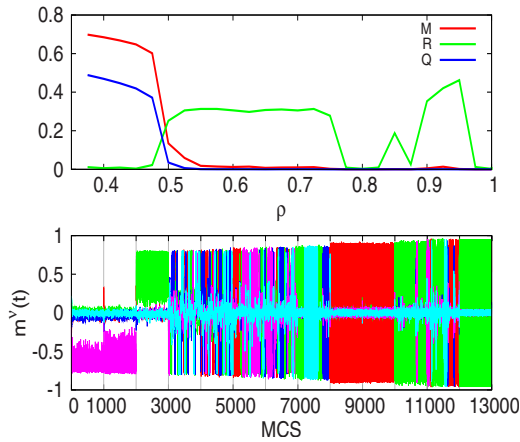


FIG. 6. (Color online) *Upper panel*: Functions $M(\rho)$, $R(\rho)$, and $Q(\rho)$ for $\Phi=-0.7$, $T=0.1$, $N=1600$, and $P=5$. (Different colors or gray intensities are here for M , R , and Q , respectively, as indicated.) *Bottom panel*: time series for the overlap functions $m^\nu(t)$ in the same case. The value of ρ is increased here during time evolution as indicated by the horizontal axis in the upper panel. (Different colors or gray intensities correspond in this graph to different values of ν .)

IV. ONSET OF IRREGULARITY

The above shows that the most intriguing behavior is when the system activity becomes irregular, e.g., as one crosses the second-order transition from the memory phase region to the nonequilibrium behavior—either at \mathbf{Ph}_4 with irregular roaming among attractors or at \mathbf{Ph}_5 where this may be randomly interrupted by series of pattern-antipattern oscillations. Figure 7 illustrates an aspect of this transition. In addition to the time evolution of some of the overlaps (right panels), which indicates where the activity is at each moment, this shows (left panels) the signal $h_i(t)$ that can sometimes be monitored in actual experiments. As a matter of

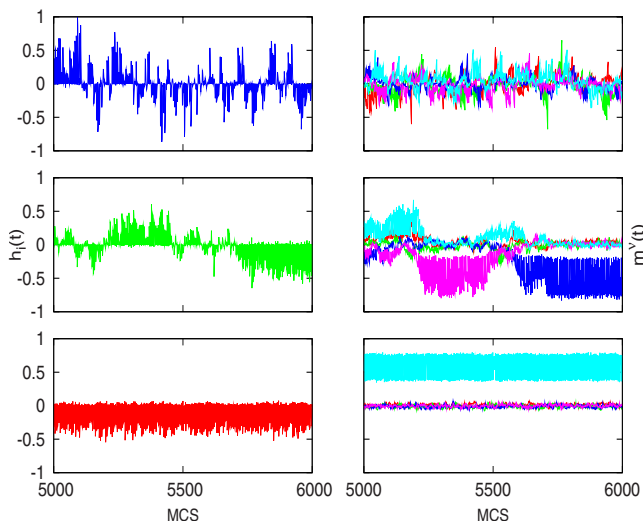


FIG. 7. (Color online) The local signal or field $h(t)$ on a typical neuron (left panels) and five overlaps $m^\nu(t)$ (right panels). These are indicated with different colors or gray intensities. The system has $N=1600$, $P=20$, $\Phi=-0.80$, $T=0.01$, and, from top to bottom, $\rho=0.225$, 0.325 (near the transition point), and 0.425 .

fact, experimentalists might find this information interesting because it is likely the data here may be compared, for instance, with electrical signals measured in single neurons—as well as more delocalized local fields—in the cortex and hippocampus of rats [49] and with magnetoencephalogram signals and recordings for single neuron action potentials [50,51].

It thus seems that it would be most interesting to characterize more quantitatively how the model signal transforms while performing the relevant transitions, that is, when moving from the case of random fluctuations around a constant value in the memory phase to the case in which the amplitude of the fluctuations increases, eventually switches to the negative of the original value, and finally reaches the case in which the frequency of switching and all the other variables become fully irregular in \mathbf{Ph}_4 and \mathbf{Ph}_5 . With this aim, we studied in detail the distribution of times of permanence in an interval around significant values of h . More specifically, in order to extract the relevant information in the case of quite different signals such as those in Fig. 7, it turned out convenient to compute the distribution of time intervals, say $\Delta\tau$, in which the signal continuously stays in any of two ranges either $h(t) > h_0$ or $h(t) < -h_0$. The cutoff h_0 intends to suppress the smallest fluctuations, which correspond to non-significant noise; this is achieved here in practice for $h_0 \in [0.05, 0.1]$. We thus observe, after averaging over the network, time, and different experiments that the interesting behavior requires relatively large systems, so that it does not occur for, say, $N=400$ and $P=5$ while it already becomes evident for, e.g., $N=6400$ and $P=40$. The most interesting fact from this study is that the exponent β in a power-law fit $\Delta\tau^{-\beta}$ monotonously increases with size from $\beta \approx 1$ for $N=800$ and $P=10$ in a way that might indicate a tendency of β to 1.5–2 (though our data that never reached this regime). These facts are illustrated in the following figures.

The left panel in Fig. 8 shows a changeover from a general exponential behavior to a power-law behavior near the interesting second-order phase transition. Analysis of the Fourier spectra reveals a similar situation, i.e., changeover from exponential to power-law behavior, concerning both the signal $h(t)$ (right panel in Fig. 8) and the overlap function $m(t)$. Figure 8 is a definite evidence for statistical criticality as one approaches the relevant transition. On the other hand, Fig. 9 shows how the system activity close to the transition between the memory equilibrium phase \mathbf{Ph}_1 and the irregular behavior in \mathbf{Ph}_4 tends to follow the power-law distribution over a larger range as one increases the size N for fixed P , which decreases α . However, we observed (not shown) that β does not depend on N , namely, the same value $\beta=1.4$ is obtained when $P=20$ for $N=1600$, 3200 , and 6400 .

V. FINAL DISCUSSION

Chemical reactions diffusing on a surface, forest fires with constant ignition of trees, parts of the nervous system vigorously reacting to weak stimuli, and the heart enduring tachycardia are paradigms of *excitable systems*—out of many cases in mathematics, physics, chemistry, and biology (see [52,53], for instance). Despite obvious differences, these sys-

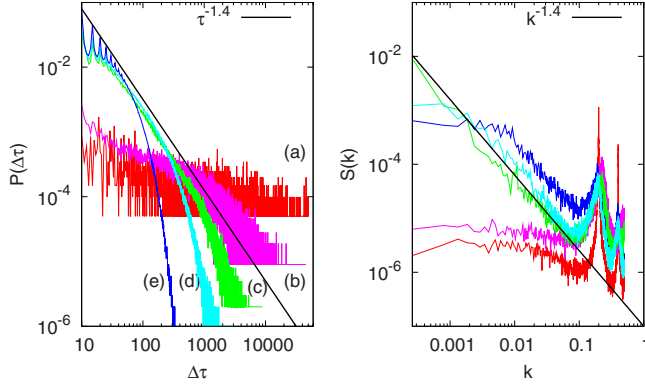


FIG. 8. (Color online) Logarithmic plots. *Left*: distribution of time intervals in which the signal continuously stays in any of the two ranges either $h(t) > h_0$ or $h(t) < -h_0$, with $h_0 = 0.1$ when $N = 1600$, $P = 20$, $\Phi = -0.8$, and $T = 0.01$ for the subcritical cases [(a) $\rho = 0.225$ —a practically horizontal signal in the \mathbf{Ph}_1 phase—and (b) 0.3], supercritical cases [(d) $\rho = 0.35$ and (e) 0.425—an exponential behavior in the \mathbf{Ph}_4 phase], and the near-critical case [(c) $\rho = 0.325$]. The latter near-critical case approximately follows the dotted line $\Delta\tau^{-\beta}$ with $\beta = 1.4$ for a large time interval. Each case corresponds to an average over 50 neurons and 20 independent systems running for 10^5 MCS. *Right*: power spectra of $h(t)$ for the same cases as in the left panel using runs with 4×10^5 MCS. The power law is illustrated with a dotted line.

tems share some characteristics. They comprise spatially distributed “excitable” units connected to each other and cooperating to allow for the propagation of signals without being gradually damped by friction. The simplest realization of the relevant excitability consists in assuming that each element has a threshold and a refractory time between consecutive responses. In order to deal with a setting which is both realistic and mathematically convenient, one may suppose that the system is networked with occasionally quiet nodes and

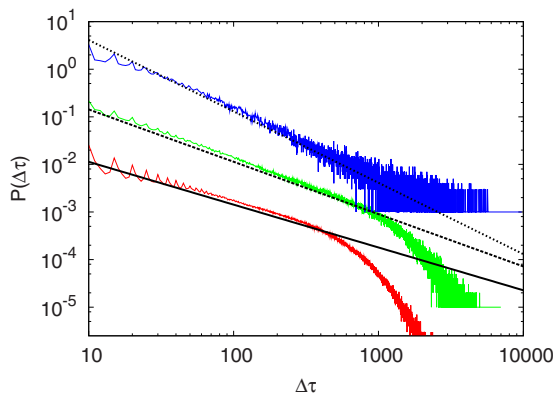


FIG. 9. (Color online) The same as in Fig. 8 to show the effect of varying the size N at fixed $\alpha = P/N = 0.003125$ and $\rho = 0.375$. From bottom to top, the data—corresponding to an average over 50 neurons and 10 independent systems—are for $N = 1600$ and 3.5×10^6 MCS (red), $N = 3200$ and 6×10^5 MCS (green), and $N = 6400$ and 8×10^4 MCS (blue). (For clarity purposes, there is a vertical translation of the data points, and it was set $h_0 = 0.05$ here.) Both the exponent β in $\Delta\tau^{-\beta}$ as well as the cutoff at which this power law fails clearly increase as N is increased.

connection weights that vary with activity on short-time scales. As a matter of fact, experimental observations reveal rest states stable against small perturbations, which correspond to the silent nodes here, and rapid varying strength of connections, either facilitating or impeding transmission, which temporarily affect thresholds and may also induce time lags during response. Furthermore, it is known that such nonequilibrium setting induces dynamic instabilities and attractors [27,44]. On the other hand, we believe that it is likely that this modeling of excitable media may, in fact, be related to the one by means of partial differential equations such as when the simple FitzHugh-Nagumo model [54] is used to represent each unit.

With this motivation, we have studied excitable media by extensive computer simulations of a discrete time model with an updated rule which generalizes the Hopfield-like standard case. The resulting phenomenology as described here is expected to describe the basic behavior in a number of apparently diverse man-made and natural excitable systems. In particular, we explicitly show how the model exhibits in the absence of stimuli highly unstable dynamics when a sufficiently large fraction ρ of nodes are “synchronized,” i.e., having their states updated, and for certain values of a noise parameter Φ that controls the noise within the connection strength. We also illustrate how these instabilities induce the occurrence of novel, first-, and second-order nonequilibrium phases. One of these happens to be most interesting as it describes the global activity wandering irregularly among a number of attractors, details strongly depending on the values of ρ and Φ . In particular, one may tune an efficient search in the model attractor space which is sensible to assume that it may be at the origin of phenomenology previously described for neural, genetic, and ill-condensed matter systems. There is also definite evidence of non-Gaussian $1/f$ noise when the system is tuned into this irregular behavior, which may explain recent experimental observations of criticality and power-law distributions in cortical networks.

Finally, we remark how the mechanism behind the irregular jumping from one pattern to the other is well understood in the model. That is, the relevant instabilities are to be directly associated to the effective local fields that one may be written as

$$h_i^{\text{eff}} \approx [1 - (1 - \Phi)\zeta(m)] \sum_{j \neq i} \omega_{ij} \sigma_j \quad (6)$$

for large N , i.e., neglecting terms of order N^{-1} . After some manipulation, one may write this more explicitly as

$$h_i^{\text{eff}} = h_i^{\text{Hebb}} - \eta \sum_{\mu} \xi_i^{\mu} (m^{\mu})^3 - \eta \sum_{(\mu \neq \nu)} \xi_i^{\mu} m^{\mu} (m^{\nu})^2. \quad (7)$$

Here, h_i^{Hebb} stands for the energy per neuron in the standard model, $\eta = (1 - \Phi)/(1 + \alpha)$, and the last sum is over all pairs of different indices μ and ν . As discussed above, h_i^{Hebb} tends to drive the system activity near the attractor associated to one of the stored patterns. Together with the second term in Eq. (7), this sums up to $\sum_{\mu} \xi_i^{\mu} m^{\mu} [1 - \eta(m^{\mu})^2]$ which, depending on the value of η , induces instabilities and irregular behavior of the overlap dynamics similar to those in a cubic map [55]. The third term in Eq. (7), on the other hand, may

be written as $-\eta \sum_{\nu} m^{\nu} h_i^{\nu}$ with $h_i^{\nu} = \sum_{\mu \neq \nu} m^{\mu} \xi_i^{\mu} m^{\nu}$. Given that ν differs from μ here, this only includes asymmetric terms $\xi_i^{\mu} m^{\nu}$ similar to those that characterize the local fields for asymmetric learning rules, namely, $\hat{h}_i = \sum_{\mu} \xi_i^{\mu} m^{\mu+1}$, which are often used to store and retrieve ordered sequences of patterns [48,56]. It is sensible to assume, therefore, that this term is most efficient in the present case in inducing transitions among patterns. Unlike for asymmetric learning [56],

however, the destabilization here does not induce any order or predictability in the sequence of visited patterns.

ACKNOWLEDGMENTS

This work was supported by the Junta de Andalucía, Project No. FQM-01505, and by the MICINN-FEDER, Project No. FIS2009-08451.

-
- [1] D. O. Hebb, *The Organization of Behavior: A Neurophysiological Theory* (Wiley, New York, 1949).
- [2] S. Amari, *IEEE Trans. Comput.* **C-21**, 1197 (1972).
- [3] J. J. Hopfield, *Proc. Natl. Acad. Sci. U.S.A.* **79**, 2554 (1982).
- [4] D. J. Amit, *Modeling Brain Function: The World of Attractor Neural Networks* (Cambridge University Press, Cambridge, 1989).
- [5] J. Marro, P. L. Garrido, and J. J. Torres, *Phys. Rev. Lett.* **81**, 2827 (1998).
- [6] J. M. Cortes, P. L. Garrido, H. J. Kappen, J. Marro, C. Morillas, D. Navidad, and J. J. Torres, *Algorithms for Identification and Categorization*, AIP Conf. Proc. No. 779 (AIP, New York, 2005), p. 178.
- [7] T. J. Wills, C. Lever, F. Cacucci, N. Burgess, and J. O'Keefe, *Science* **308**, 873 (2005).
- [8] M. Rabinovich, R. Huerta, and G. Laurent, *Science* **321**, 48 (2008).
- [9] M. O. Magnasco, O. Piro, and G. A. Cecchi, *Phys. Rev. Lett.* **102**, 258102 (2009).
- [10] T. Petermann, T. C. Thiagarajan, M. Lebedev, M. Nicolelis, D. R. Chialvo, and D. Plenz, *Proc. Natl. Acad. Sci. U.S.A.* **106**, 15921 (2009).
- [11] E. Thelen and L. B. Smith, *A Dynamic Systems Approach to the Development of Cognition and Action* (The MIT Press, Cambridge, MA, 1994).
- [12] W. J. Freeman, *Neural Networks* **13**, 11 (2000).
- [13] H. Korn and P. Faure, *C. R. Biol.* **326**, 787 (2003).
- [14] K. Kaneko and I. Tsuda, *Chaos* **13**, 926 (2003).
- [15] J. S. Perkimki, T. H. Makikallio, and H. V. Huikuri, *Clin. Exp. Hypertens.* **27**, 149 (2005).
- [16] M. Shen, G. Chang, S. Wang, and P. J. Beadle, *Lecture Notes in Computation Science* **3973**, 560 (2006).
- [17] L. M. Jones, A. Fontanini, B. F. Sadacca, P. Miller, and D. B. Katz, *Proc. Natl. Acad. Sci. U.S.A.* **104**, 18772 (2007).
- [18] M. I. Rabinovich and M. K. Muezzinoglu, *Phys. Usp.* **53**, 357 (2010).
- [19] H. Sompolinsky, A. Crisanti, and H. J. Sommers, *Phys. Rev. Lett.* **61**, 259 (1988).
- [20] M. Adachi and K. Aihara, *Neural Networks* **10**, 83 (1997).
- [21] H. Bersini and P. Sener, *Neural Networks* **15**, 1197 (2002).
- [22] H. Lu, *Phys. Lett. A* **298**, 109 (2002).
- [23] X. S. Yang and Q. Yuan, *Neurocomputing* **69**, 232 (2005).
- [24] W. Freeman and M. D. Holmes, *Neural Networks* **18**, 497 (2005).
- [25] C. Molter, U. Salihoglu, and H. Bersini, *Neural Comput.* **19**, 80 (2007).
- [26] W.-Z. Huang and Y. Huang, *Appl. Math. Comput.* **206**, 1 (2008).
- [27] J. Marro, J. J. Torres, and J. M. Cortes, *J. Stat. Mech.: Theory Exp.* (2008), P02017.
- [28] J. J. Torres, J. Marro, J. M. Cortes, and B. Wemmenhove, *Neural Networks* **21**, 1272 (2008).
- [29] O. Mazor and G. Laurent, *Neuron* **48**, 661 (2005).
- [30] J. Marro and R. Dickman, *Nonequilibrium Phase Transitions and Critical Phenomena in Lattice Systems* (Cambridge University Press, Cambridge, 2005).
- [31] J. J. Torres, P. L. Garrido, and J. Marro, *Phys. Rev. B* **58**, 11488 (1998).
- [32] Y. Bar-Yam, D. Harmon, and B. de Bivort, *Science* **323**, 1016 (2009).
- [33] O. Hallatschek and D. R. Nelson, *Phys. Today* **62**(7), 42 (2009).
- [34] A. Diaz-Guilera and E. R. Alvarez-Buylla, in *Handbook on Biological Networks*, Lecture Notes in Complex Systems, edited by S. Boccaletti, V. Latora, and Y. Moreno (World Scientific, Singapore, 2009), Vol. 10.
- [35] J. T. Sun, S. J. Wang, Z. G. Huang, L. Yang, Y. Do, and Y. H. Wang, *New J. Phys.* **12**, 063034 (2010).
- [36] D. R. Chialvo, *Physica A* **340**, 756 (2004).
- [37] V. M. Eguíluz, D. R. Chialvo, G. A. Cecchi, M. Baliki, and A. V. Apkarian, *Phys. Rev. Lett.* **94**, 018102 (2005).
- [38] W. J. Freeman, M. D. Holmes, A. West, and S. Vanhatalo, *Clin. Neurophysiol.* **117**, 1228 (2006).
- [39] D. R. Chialvo, P. Balenzuela, and D. Fraiman, *Collective Dynamics: Topics on Competition and Cooperation in the Biosciences* (AIP, New York, 2008).
- [40] J. A. Bonachela, S. de Franciscis, J. J. Torres, and M. A. Muñoz, *J. Stat. Mech.: Theory Exp.* (2010), P02015.
- [41] D. Plenz and D. Chialvo, e-print arXiv:0912.5369.
- [42] D. Millman, S. Mihalas, A. Kirkwood, and E. Niebur, *Nat. Phys.* **6**, 801 (2010).
- [43] J. J. Hopfield, *Proc. Natl. Acad. Sci. U.S.A.* **81**, 3088 (1984); W. S. McCulloch and W. Pitts, *Bull. Math. Biophys.* **5**, 115 (1943); M. E. J. Newman, *SIAM Rev.* **45**, 167 (2003); S. Boccaletti, V. Latora, Y. Moreno, M. Chavez, and D. U. Hwang, *Phys. Rep.* **424**, 175 (2006).
- [44] S. Johnson, J. Marro, and J. J. Torres, *EPL* **83**, 46006 (2008).
- [45] J. M. Cortes, J. J. Torres, J. Marro, P. L. Garrido, and H. J. Kappen, *Neural Comput.* **18**, 614 (2006).
- [46] J. Mejias, H. Kappen, and J. Torres, e-print arXiv:1007.3556, PLoS One (to be published).
- [47] D. J. Amit, H. Gutfreund, and H. Sompolinsky, *Phys. Rev. Lett.* **55**, 1530 (1985); *Phys. Rev. A* **32**, 1007 (1985).
- [48] M. Griniasty, M. V. Tsodyks, and D. J. Amit, *Neural Comput.*

- [5](#), [1](#) (1993).
- [49] J. Csicsvari, D. A. Henze, B. Jamieson, K. D. Harris, A. Sirota, P. Baethó, K. D. Wise, and G. Buzsáki, *J. Neurophysiol.* **90**, [1314](#) (2003).
- [50] M. Hämmäläinen, R. Hari, R. J. Ilmoniemi, J. Knuutila, and O. V. Lounasmaa, *Rev. Mod. Phys.* **65**, [413](#) (1993).
- [51] See, however, Ref. [18] for an important concern on temporal and spatial resolutions.
- [52] D. Kaplan and L. Glass, *Understanding Nonlinear Dynamics* (Springer, New York, 1995).
- [53] E. M. Izhikevich, *Dynamical Systems in Neuroscience: The Geometry of Excitability and Bursting* (MIT Press, Cambridge, MA, 2007).
- [54] R. FitzHugh, *Bull. Math. Biophys.* **17**, [257](#) (1955); *Biophys. J.* **1**, [445](#) (1961); J. Nagumo, S. Yoshizawa, and S. Arimoto, *IEEE Trans. Commun. Technol.* **12**, [400](#) (1965).
- [55] T. D. Rogers and D. C. Whitley, *Math. Modell.* **4**, [9](#) (1983).
- [56] J. Hertz, A. Krogh, and R. G. Palmer, *Introduction to the Theory of Neural Computation* (Addison-Wesley, Reading, MA, 1991).